Int. J. Electrochem. Sci., 8 **(2013)** 5698 - 5709

International Journal of
ELECTROCHEMICAL
SCIENCE
www.electrochemsci.org

Phenol Degradation Using Glassy Carbon Electrodes Modified with Particles of Co-Mo Alloy

S. I. Orozco[1], *L.M. Blanco*[1 *], *M. A. Garza*[2], *V. A. González*[2], *C. Borrás*[3], *B. Sharifker*[3].

[1] Universidad Autónoma de Nuevo León, Facultad de Ciencias Químicas, Laboratorio de Electroquímica. Guerrero y Progreso S/N, Col. Treviño, Monterrey, N. L., México, CP 64570.
[2] Universidad Autónoma de Nuevo León, Centro de Innovación, Investigación y Desarrollo en Ingeniería y Tecnología. Avenida Alianza 101 Sur, PIIT Monterrey, Apodaca, N. L., México, CP 66600
[3] Universidad Simón Bolívar, Laboratorio de Electroquímica. Valle de Sartenejas, Baruta, Edo. Miranda, Edf. Q y P, PB, Ofic. 10, Caracas, Venezuela, Apartado postal 89000.
[*]E-mail: leonyjerez@gmail.com

Received: 16 February 2013 / *Accepted:* 13 March 2013 / *Published:* 1 April 2013

This paper reports on a study aimed to modify the surface of glassy carbon (VC) with Co-Mo nanoparticles and to determine their morphology and composition in order to evaluate their electrocatalytic activity for degrading phenol. The electrochemical deposition of Co-Mo from $CoSO_4$ and Na_2MoO_4 in two molar relations (Co:Mo 2.3:1 and 20:1) was analyzed. Experiments were conducted in a conventional three-electrode cell using glassy carbon as the working electrode (WE), Ag/AgCl(s) as the reference electrode (RE) and Pt as the auxiliary electrode (CE). A citrate bath at pH 6 was used as supporting electrolyte. The electrode modification was carried out potentiostatically at –1.1 V vs. $Ag/AgCl_{(s)}$ and galvanostatically at –0.003 A/cm^2. The modified electrodes were characterized by XRD, TEM and XPS. Analyses showed that the obtained deposits were a mixture of Co_2Mo_3 alloy and $CoMoO_3$ oxide. The ability of the electrode modified with Co-Mo particles to degrade phenol was studied. Degradation rate was 95% in 3 hours on a synthetic solution of phenol 30 ppm. UV-Vis spectra of the solutions obtained during electrochemical phenol reduction allowed identifying benzene and cyclohexane as the reaction products.

Keywords: Electrode modification, potentiostatic deposition, bimetallic materials, mixed compounds, phenol degradation.

1. INTRODUCTION

Phenols and substituted phenolic compounds in natural waters have toxic effects on humans, animals and plants and they cause undesirable taste and odor in drinking water, even at low

concentrations. For these reasons, many phenolic compounds have been included in environmental legislations [1].

These compounds are released to the environment by many industries, such as pharmaceutical plants, oil refineries and coke plants. They pose great risk to environmental ecology and public health. Most phenols are recalcitrant to the conventional physicochemical and biological treatments [2, 3].

Phenol is considered a model pollutant; it is typically found in effluents from oil, textile, painting, pesticide, dye and pharmaceutical industries. Aromatic compounds are generally toxic and those having a quinone structure exhibit very high toxicity. Removing phenol from aqueous effluents by liquid-liquid extraction for concentrations below 4,000 ppm is not economically viable. Furthermore, biological processes are slow (last more than 21 h) at concentrations above 5 ppm [2, 4]. Hence, other techniques are needed to destroy this pollutant.

Electrochemical techniques that allow reducing the quantity of organic pollutants in solution are: separation by electrofloculation [5, 6]; oxidation by electrogenerated Fenton's reagent [3, 7–9], among others. The complete oxidation of phenol in aqueous solution by electrochemical means has been carried out on anode materials such as PbO_2 [10], WO_3 [11, 12] and BDD [4, 13–18].

Electrochemical deposition is a good technique to prepare highly functional catalytic surfaces. Different alloys can be electrodeposited to increase the electrocatalytic activity of the electrode [19, 20]. For example, Kuznetsov *et al.* found that the rate of hydrogen evolution in 1 M NaOH at 293 K for the Co-Mo alloy is higher than that for pure cobalt deposits obtained in similar conditions. This higher rate is due to the increase of the electrode true surface area and possibly also to the electronic structure of the obtained alloys [21, 22]. Gómez *et al.* studied the influence of pH on the Co-Mo deposits. The electrolyte pH produced a considerable effect on the deposit morphology (pH 8 produced powder-like deposits) [20]. Sidel'nikova *et al.* also studied the possibility of obtaining cobalt-molybdenum coatings at room temperature from a citrate electrolyte containing an additional complexing agent—EDTA sodium salt [23].

Electrode surfaces modified with Co-Mo alloys have also shown interesting magnetic properties [20] and can be applied in fuel cells [21, 22]. Direct degradation of organic compounds requires modified electrodes and electrodeposition is a good technique to prepare them [20, 24–27]. Different alloys can be electrodeposited to obtain nanoparticle films with useful electrocatalytic properties. In particular, Co-Mo can be used because of its properties [21, 22], which depend on the molybdenum percentage.

Gomez *et al.* studied the Co-Mo deposition process and showed that electrodeposition is a suitable method for preparing alloys that contain cobalt and molybdenum [24–27]. Moreover, the electrodeposition of molybdenum with iron-group metals has been gaining importance in recent years due to the high electrocatalytic properties of these metals in the hydrogen evolution reaction (HER) [21, 22]. The Co-Mo system is an example of induced codeposition. Molybdenum has not been deposited alone from an aqueous solution [20], but only codeposited with another metal. Induced molybdenum codeposition with iron-group metals has been achieved [20, 23–25]. Knowledge of the induced discharge process is essential to correlate the properties of the coatings to the conditions of their deposition. The presence of polycarboxylate is required to obtain molybdenum codeposits with iron-group metals [24–26].

This paper reports on the glassy carbon electrode modification with particles of cobalt and molybdenum, its characterization and the deposit's electrocatalytic activity in the phenol reduction in an alkaline solution.

2. EXPERIMENTAL

All chemicals used were analytical grade ($CoSO_4 \cdot 7H_2O$, $Na_2MoO_4 \cdot 2H_2O$, and sodium citrate ($Na_3C_6H_5O_7 \cdot 2H_2O$)). Solutions were freshly prepared with nanopure water. Before experiments, solutions were de-aerated with nitrogen. Working solutions were: 1) S1: $CoSO_4$ (100 mM) and Na_2MoO_4 (5 mM); 2) S2: $CoSO_4$ (100 mM) and Na_2MoO_4 (43 mM); 3) S3: $CoSO_4$ (100 mM). Sodium citrate (200 mM) was used as the supporting electrolyte for both solutions. Working pH was 6.0 and the temperature was maintained at 25°C.

Cyclic voltammetry was used to determine the conditions of nucleation and growth of Co-Mo deposits. The reference electrode was $Ag/AgCl_{(s)}$ and all potentials are referred to this electrode. Chronoamperometry (at –1.1 V) and chronopotentiometry (at –0.003 A/cm^2) were used to modify the surface with the Co-Mo alloy.

The deposit morphology was examined with a FEI Titan field emission gun TEM. Elemental composition was determined with an X-ray analyzer. X-ray diffraction (XRD) phase analysis was performed in a Philips MRD diffractometer in low-resolution parallel beam optics. Diffractograms were obtained in the 10–90 2θ range, with a 0.05° step and a measuring time of 5 s per step. The chemical state of the films was studied by X-ray photoelectron spectroscopy (XPS), with a PHI 5600 multi-technique system, using standard Al Kα radiation with a resolution of 0.1 eV. The take-off angle relative to the substrate was 45°. Charging effects were corrected by referring the binding energies to that of the C1s line at 284.8 eV.

Electrolysis at constant potential was carried out with an Autolab PGSTAT 30 potentiostat. Measurements were conducted using a 40 mL three-compartment glass cell with a glass frit separating the working and counter electrode compartments. The electrodes modified with Co-Mo alloy particles were used as working electrodes (surface/volume ratio of 0.025 cm^{-1}) and a large-area platinum gauze and $Ag/AgCl_{(s)}$ were used as auxiliary and reference electrodes, respectively. Phenol degradation was studied by UV-Vis absorbance spectra using a Cary 100 Varian spectrophotometer and scanning in the region between 200 and 500 nm.

3. RESULTS AND DISCUSSION

3.1. Voltammetric results

The electrochemical behavior of Co-Mo deposition was analyzed by voltammetric experiments. The blank solution response was recorded; no processes take place between –1.2 V and 1.2 V.

Fig. 1 depicts the voltammetric response of the glassy carbon electrode in the S1 and S2 solutions. Fig. 1 also shows the typical nucleation loop in the reduction zone that reveals the deposition process.

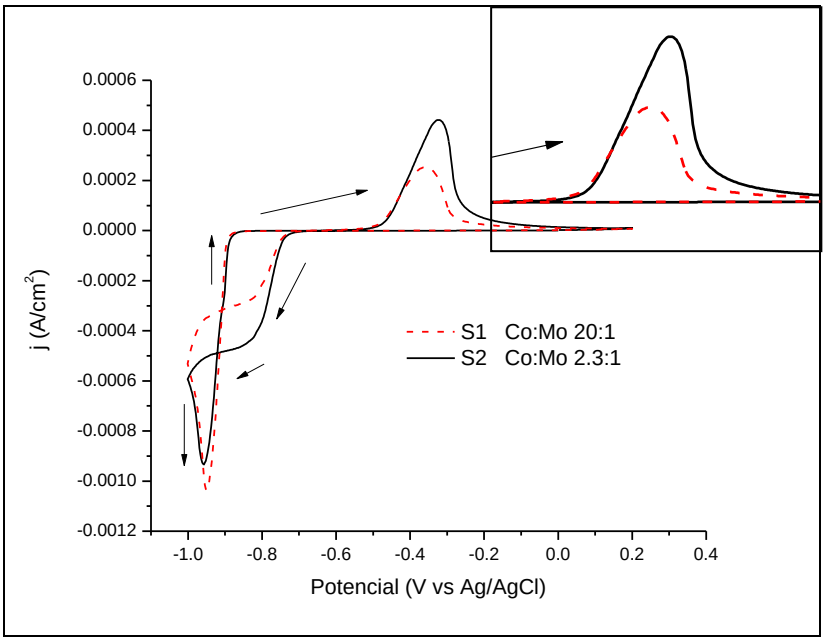

Figure 1. Cyclic voltammograms of the glassy carbon electrode in the S1 (dashed line) and S2 (solid line) solutions, pH 6, 50 mV/s scan rate

For the S2 solution, the voltammogram shows that the higher the molybdate content in solution, the higher the cathodic current. Hence, increasing the molybdate content enhances the deposition adherence. Fig. 1 also shows that the redox process is similar in the S1 and S2 solutions. Alloy deposition started at approximately –1 V in both solutions. In the positive scan, a complex oxidation peak was observed in both solutions around –0.4 V. This peak suggests the formation of intermetallic phases corresponding to the alloy formation [24–27].

An increase of the molybdate concentration to Co:Mo 2.3:1 from Co:Mo 20:1, causes the primary layer of molybdenum oxides to become thicker according to the electrodeposition mechanism. Since the molybdenum oxides are semiconductors, the increase in thickness shifts the onset of alloy deposition to more negative potentials, at which deposition is accompanied by hydrogen evolution [28].

3.2. Electrode modification

Electrode modification by electrodeposition was carried out potentiostatically and galvanostatically.

Chronoamperometry (CA) was selected as the Co-Mo electrodeposition method because of the interest in having nanoparticles on the surface of the electrodes. A deposition potential of –1.1 V was selected because deposition potentials higher than –0.8 V favor only the formation of molybdenum

oxides [20, 25], whereas more negative deposition potentials induce hydrogen evolution, damage the deposit and favor bubble formation on the electrode surface [28].

With this electrochemical method, the electrodeposition process shows the nucleation and growth phases at –1.1 V in the S1 and S2 solutions (Fig. 2). The nucleation process took place in less than 30 s, but the step time was extended to 300 s to allow the growth of deposits. The modified electrode obtained from the S1 solution was CA1 and the one obtained from the S2 solution was CA2.

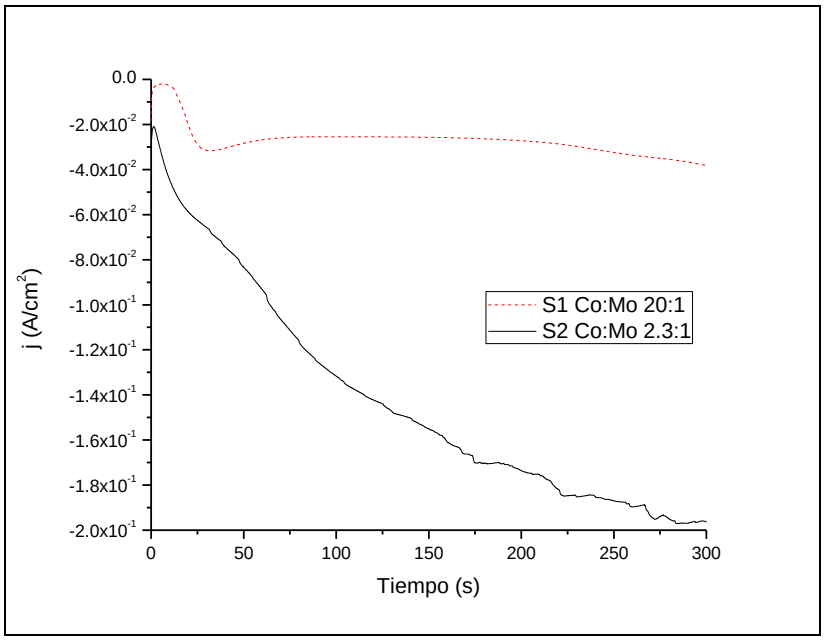

Figure 2. Chronoamperometry of the glassy carbon electrode in the S1 (dashed line) and S2 (solid line) solutions, pH 6, E = –1.1 V, t = 300 s

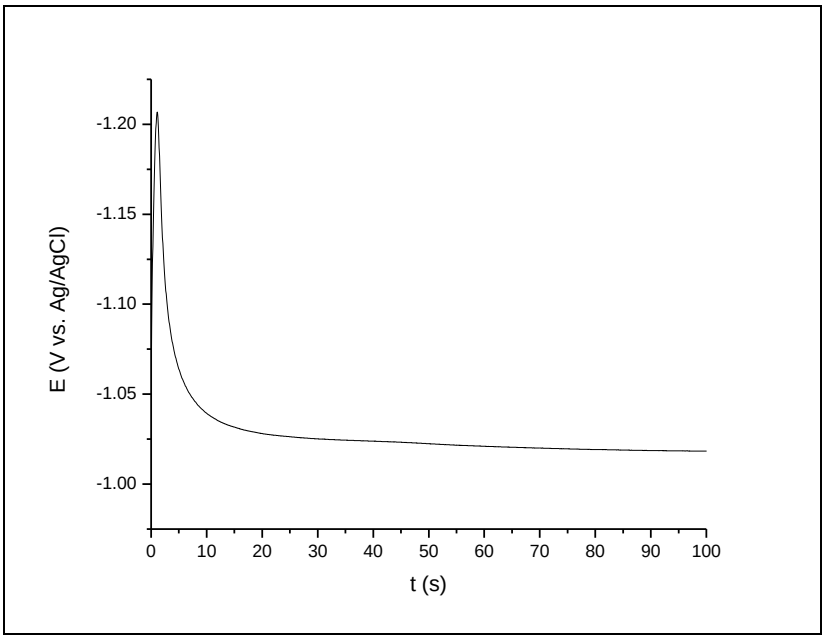

Figure 3. Chronopotenciometry of the CP2 electrodeposition, –0.003 A/cm^2, 300 s, pH 6

Chronopotenciometry was carried out in the same solutions as those used for the CA2 deposit to study the effect of applying this technique on the morphology and composition of the deposit; the modified electrode obtained was CP2. Chronopotentiometry was performed applying a current density of –0.003 A/cm^2. The electrochemical process (Fig. 3) shows an initial potential jump that indicates the nucleation on the electrode surface, and later a stabilization of the potential that defines the stage of nuclei growth. The growing potential was close to –1.025 V.

3.3. Electrode characterization

The CA2 and CP2 modified electrodes were characterized by XRD, TEM and XPS. XRD was used to determine the phases present on the electrode surface (Fig. 4). TEM was used to determine the predominant phase (Fig. 5) [29]. XPS was used to confirm the existence of an intermetallic Co-Mo bond on the electrode surface.

Fig. 4 depicts the result of the XRD analysis of CA2 and CP2. The obtained diffraction patterns suggest that both samples have a composition based on the Co_2Mo_3, $CoMoO_3$, $CoMo_3O_8$ and Co_7O_6 phases, as it has been reported in the literature [see JCPDS: 29-0490, JCPDS 21-0869JCPDS:34-0511 and JCPDS: 29-0489].

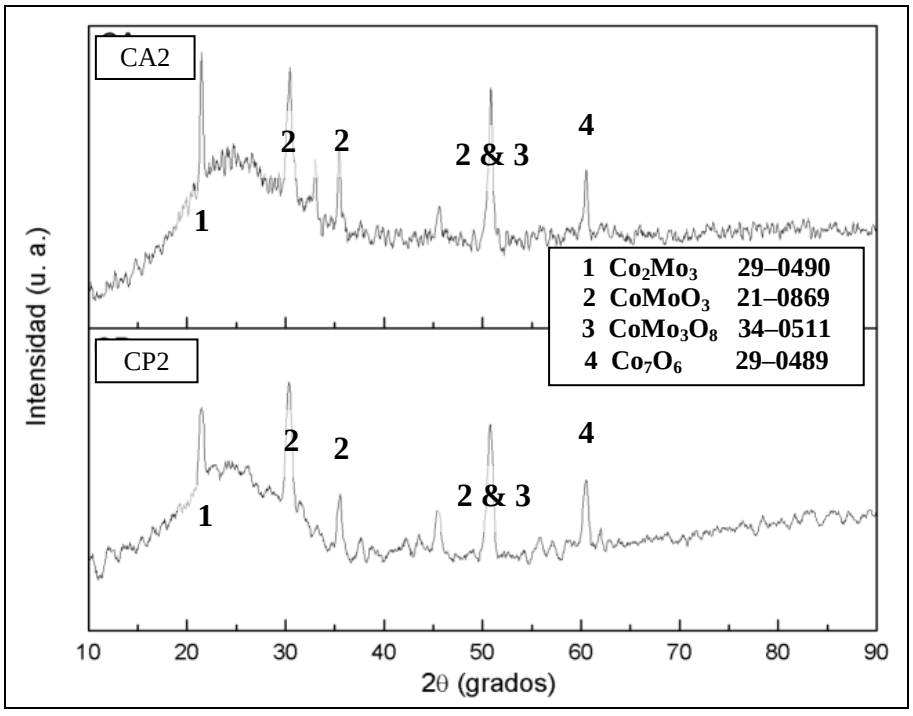

Figure 4. XRD analysis of CA2 and CP2, 10–90 2θ, 30 min

In order to corroborate these characteristics on our samples, we analyzed them by TEM. Figure 5 summarizes the crystalline and morphological characteristics of the samples. Figure 5a shows well-dispersed nanoparticles with diameters of 5–10 nm. It also shows particle agglomeration in some

regions, which can be attributed to the formation mechanism of an intermetallic induction [27]. Moreover, Figures 5b and 5c show that the crystalline arrangement corresponds to the Co_2Mo_3 phase, since the measured interplanar distance of 2.6 Å can be related to the distance between the planes of the Co_2Mo_3 and $CoMoO_3$ families. Figure 5d, which depicts selected area electron diffraction (SAED) of CA2, shows the presence of a mixture of phases. The analysis revealed diffraction spots, attributable to planes of the Co_2Mo_3 and $CoMoO_3$ families according to the measures of 0.2702, 0.2714 and 0.1521 nm corresponding to mixed oxides of Co and Mo. These diffractions correspond to a $CoMoO_3$ DRX structure, but there is also an r = 0.2879 diffraction that corresponds to the formation of the Co_2Mo_3 29-0490 alloy.

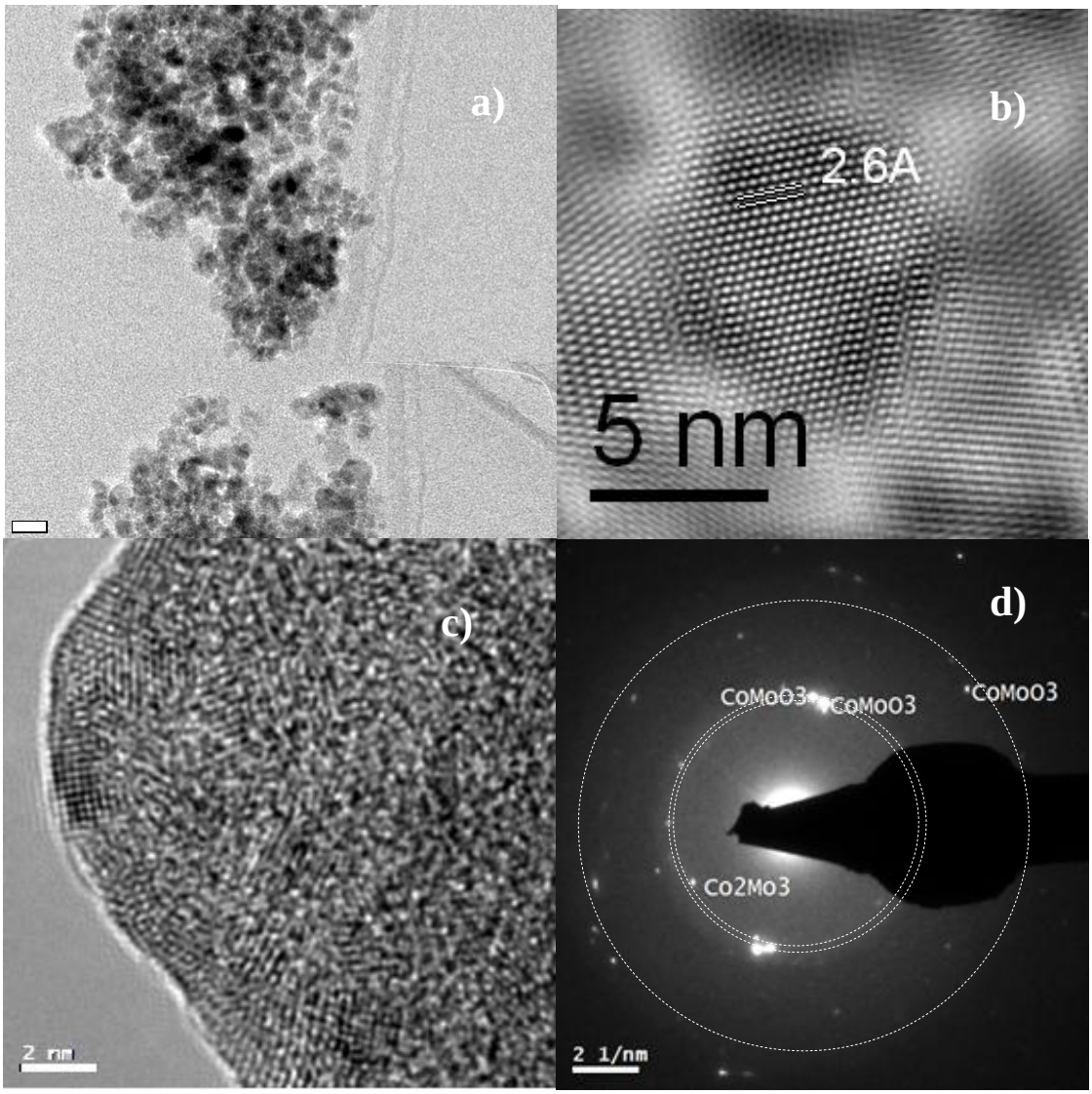

Figure 5. Two-dimensional view of TEM images and SAED: a) CA2, 8700X, beam energy of 300 keV; b) CA2, 10000X, beam energy of 300 keV; c) CP2, 10000X, beam energy of 300 keV; d) SAED of CA2

XRD and SAED analyses showed the presence of Co_2Mo_3, but an XPS analysis was necessary to confirm the alloy electrodeposition.

XPS analysis of CA2 (Fig. 6) revealed a $3d_{5/2}$ peak at 228.02 eV, a $3d_{3/2}$ peak at 231.15 eV, and a 3.13 eV difference between the $3d_{3/2}$ and $3d_{5/2}$ peaks. These values correspond to Mo^0 [30]. In the electrodeposition of anomalous alloys (a mechanism reported in the literature [20, 27]), such as that of the Co-Mo alloy, the electrodeposition of molybdenum requires an induction process. For this reason, the presence of Mo^0 confirms the Co_2Mo_3 alloy formation.

All the performed analyses confirm the presence of mixed phases on the modified electrode surface. These mixed phases result from the Co-Mo alloy and mixed oxides. The formation of these mixed oxides was favored by the molybdate concentration increase.

As in any induced intermetallic deposition, a molybdenum oxide film was formed on the electrode and then the Co-Mo nanoparticles grew over this film.

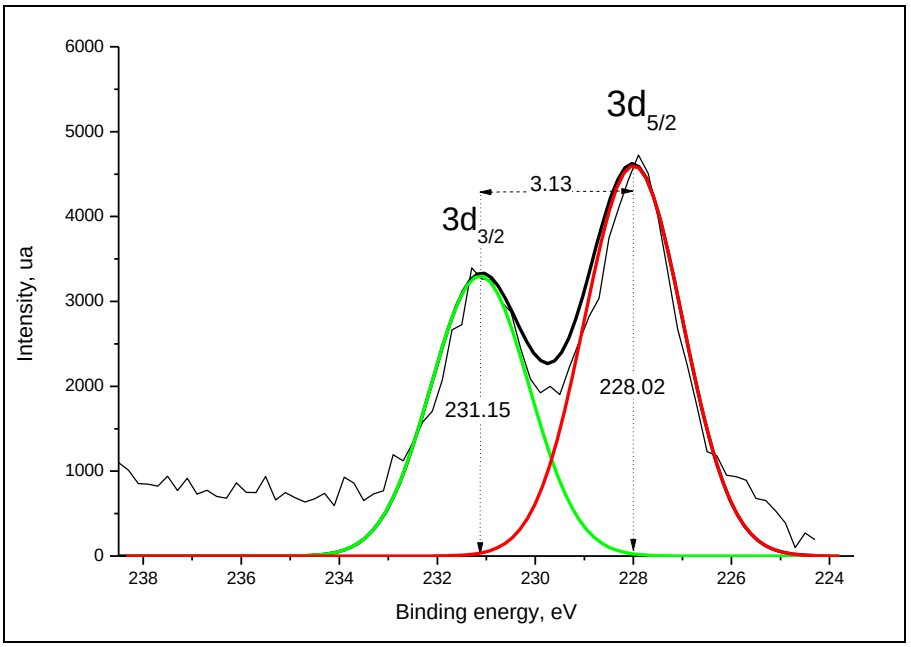

Figure 6. XPS analysis of CA2, 224–238 eV binding energy

3.4. Phenol degradation

Bulk electrolysis of 30 ppm phenol solutions was carried out to determine the phenol degradation by reduction using different modified electrodes (different deposit compositions). Table 1 shows the electrodeposition conditions. Glassy carbon was used as the WE; the electrode modifications were carried out in steps of –1.1 V during 300 s; the controlled-potential electrolysis was performed at –1.21 V for 180 min; the phenol concentration decrease was monitored by UV-Vis spectra at 269 nm. Electrodes modified with deposits of pure cobalt, Co_2Mo_3 + $CoMoO_3$ (CA2) and Co-Mo (CA1) were used to degrade phenol by cathodic reduction. The best result corresponds to CA2, which has the highest molybdenum concentration. According to the electrolysis data, this electrode has a good electrocatalytic activity to remove phenol by reduction.

Figure 7 depicts the bulk electrolysis results and shows the significant increase of electrocatalytic activity of the CA2 modified electrode, which removes 94.87% of the phenol in 180 min. According to the literature, the presence of cobalt molybdenum oxide in the CA2 electrode surface can increase its electrocatalytic activity because of the synergistic effect between Co and Mo [31, 32].

The synergic effect between Co and Mo can be attributed to the mechanism of electrochemical formation of an anomalous by induction alloy, such as the Co-Mo alloy.

Table 1. Modified electrode electrodeposition conditions

Modified electrode designation	Electrodeposition Solutions Co:Mo	Composition
CACo	S3 (100 mM:0 mM)	Pure cobalt
CA2	S2 (2.3:1)	$Co_2Mo_3 + CoMoO_3$
CA1	S1 (20:1)	Co-Mo

On the other hand, the CA1 modified electrode, which contains less molybdenum than CA2, does not provide a significant improvement over the pure cobalt electrode in 180 min.

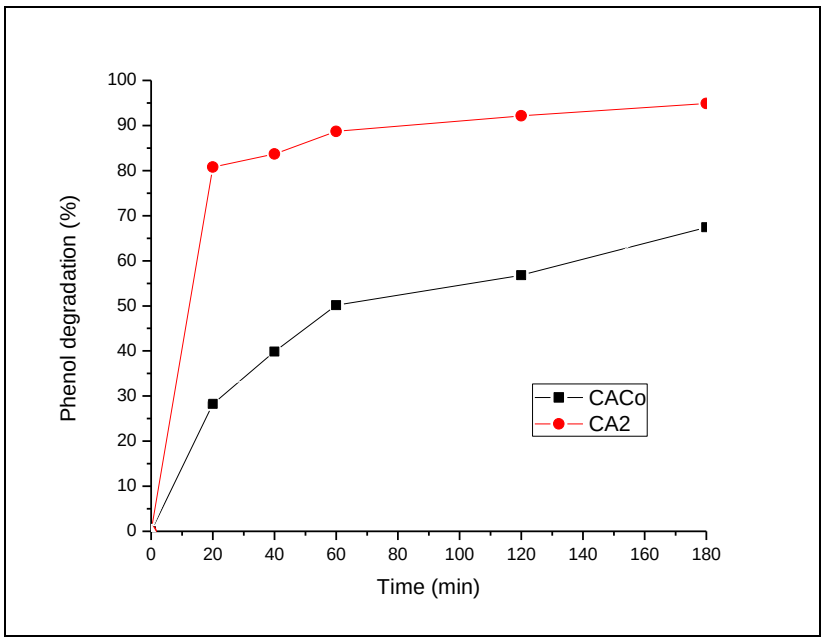

Figure 7. Bulk electrolysis results using different modified electrodes

The mechanism of the Co-Mo alloy formation by electrodeposition suggests the electrolytic formation of a molybdenum oxides layer; these oxides chemically react with the electrochemically reduced cobalt to form the Co-Mo bond [24–27].

In addition, Kuznetsov et al. [21] showed the electrocatalytic capability of the deposits of this alloy on vitreous carbon in the hydrogen evolution reaction; they found that increasing the amount of molybdenum in the alloy has a favorable effect on this reaction.

Considering the previous analysis, we conclude that the exhaustive electrolysis of phenol over an electrode modified with the Co-Mo alloy (Co2Mo3) and the CoMoO3 oxide occurs together with an electrocatalytic hydrogen generation that facilitates the pollutant reduction.

On the other hand, the CA1 modified electrode, which contains less molybdenum than CA2, does not provide a significant improvement over the pure cobalt electrode in 180 min.

Table 2 summarizes the phenol degradation percentages for different electrodes. These data show that the CA2 electrode provides a degradation of 94.87% for 180 min. The standard deviation for this value was ±1.86 %. This degradation is higher than the 67.44% degradation obtained with CACo (pure cobalt) for 180 min.

Table 2. Phenol degradation percentages for different modified electrodes

Time (min)	CACo	CA1	CA2
	Cobalt	Co-Mo	Co_2Mo_3 + $CoMoO_3$
	Degradation (%)		
0	0	0	0
20	28.24	31.89	80.77
40	39.87	34.88	83.68
60	50.17	38.87	88.70
120	56.81	47.52	92.15
180	67.44	74.42	94.87

Bulk electrolysis results also revealed that phenol degradation mainly occurs during the first 20 min of reaction. After 180 min, there was no significant degradation even if the electrolysis was extended to 300 min.

During bulk electrolysis using the CA2 modified electrode, an immiscible organic phase appears. Further UV-Vis analysis of the aqueous solution between 200 and 500 nm (Fig. 8) showed the formation of two reaction byproducts. UV-Vis spectra showed one absorption band at 210 nm and a group or bands at 260 nm. According to [33–35], the first band corresponds to cyclohexane and the group of bands corresponds to benzene.

To confirm the presence of cyclohexane and benzene a blank solution containing water, sodium citrate 0.2 M, phenol 30 ppm, benzene 0.001 L and cyclohexane 0.001 L was prepared. Figure 8 shows the UV-Vis spectra of this solution and that of the bulk electrolysis final solution. The results revealed that the reaction products were in fact cyclohexane and benzene.

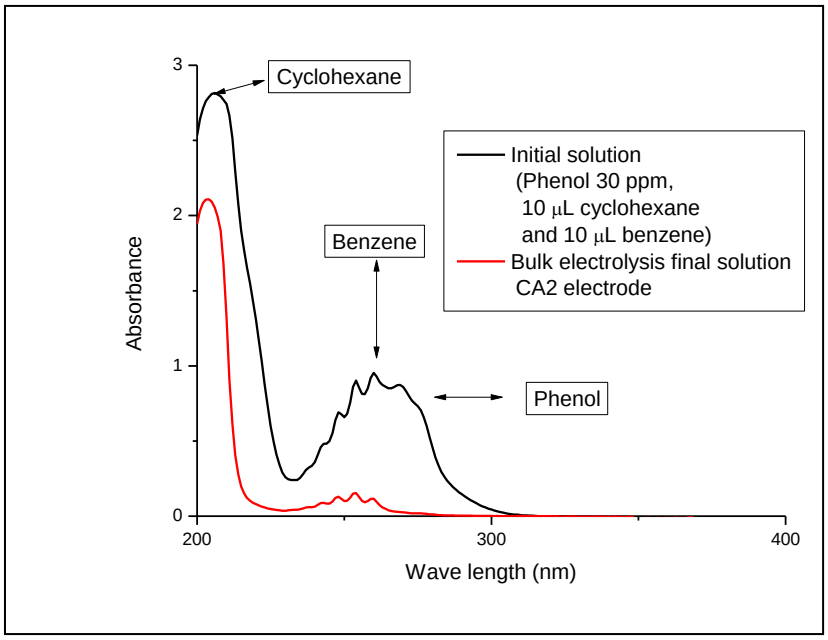

Figure 8. UV-Vis spectra of the solution (phenol 30 ppm and 0.001 mL of benzene and cyclohexane as blank solution) and of the bulk electrolysis final solution.

4. CONCLUSIONS

Glassy carbon electrodes, modified by electrodeposited nanoparticles of a mixture of Co_2Mo_3 and $CoMoO_3$ (CA2) have electrocatalytic activity for phenol reduction. These electrodes degrade phenol in synthetic solutions of phenol 30 ppm.

Bulk electrolysis of phenol with the CA2 working electrode having a surface/volume ratio of 0.025 cm^{-1}, at –1.2 V vs. $Ag_{(s)}$/AgCl, removed approximately 95% of phenol in 3 h.

ACKNOWLEDGMENT
We gratefully acknowledge Dr. Wencel de la Cruz (Centro de Nanociencias y Nanotecnología, Universidad Autónoma de México) for his support in the XPS analyses. This research project was financially supported by PAICYT (Project IT161-09).

References

1. T. Ndlovu, O. Arotiba, R. Krause, B. Mamba, *Int. J. Electrochem. Sci.*, 5 (2010) 1179.
2. X, Zhenga, M. Ernstb, M. Jekela, Water Research, 44 (2010) 3203.
3. L. Jiang, X. Mao, *Int. J. Electrochem. Sci.*, 7 (2012) 4078.
4. E. Weiss, K. Groenen-Serrano, A. Savall, *J. of Appl. Electrochemistry*, 38 (2007) 329.
5. G. Ciardelli and G. Ranieri, *Wat Res*, 35 (2001) 56.
6. A. Cerqueira, C. Russo, M. Marques, *Brazilian J. of Chem. Eng.*, 26, (2009) 659.
7. B. Gözmen, M. Oturan, N. Oturan, O. Erbatur, *Environ. Sci. Tech.*, 37 (2003) 3716.
8. E. Brillas, M. Baños, M. Skoumal, P. Cabot, J. Garrido, M. Rodríguez, *Chemosphere*, 68 (2007) 199.
9. S. Ammar, N. Oturan, M. Oturan, *J. Environ. Eng. Manage*, 17 (2007) 89.
10. S. Abaci, U. Tammer, K. Pekmez, A. Yildiz, *Appl. Surf. Sci.*, 240 (2005) 112.

11. H. Habazaki, Y. Hayash, H. Konno, *Electrochim Acta*, 47 (2002) 4181.
12. D. Su, J. Wang, Y. Tang, Ch. Liu, L. Liu, X. Han, *Chem. Commun*, 47 (2011) 4231.
13. A. Polcaro, M. Mascia, S. Palmas, *Annali di Chimica*, 93 (2003) 967.
14. J. Iniesta, P. Michaud, M. Panizza, *Electrochim Acta*, 46 (2001) 3573.
15. P. Cañizares, J. Lobato, R. Paz, *Wat. Res*., 39 (2005) 2687.
16. M. Panizza, G. Cerisola, *Electrochimica Acta*, 51 (2005) 191.
17. E. Weiss, G. Serrano, A. Savall, Ch. Comninellis, *J. Appl. Electrochem*., 37 (2005) 41.
18. G. Palma, F. Guzmán-Duque, G. Peñuela, *Chemosphere*, 81 (2010) 26.
19. A. Wieckwowski, *Catalysis and Electrocatalysis at nanoparticles surfaces*, Taylor and Francis e-Library, New York (2009).
20. E. Gómez, Z. Kipervaser, E. Vallés, *J. of Applied Electrochem.*, 33 (2003) 245.
21. V. Kuznetsov, A. Kalinkina, T. Pshenichkina, V. Balavaev, *Russian J. of Electrochem.*, 44 (2008) 1350.
22. V. Kuznetzov, Z. Bondarenko, T. Pshenichkina, N. Morozova, V. Kudryavtsev, *Russian J. of Electrochem*., 43 (2007) 349.
23. S. Sidel'nikova, G. Volodina, D. Grabko, A. Dikusar, *Surface Eng. and Appl. Electrochem*., 43 (2007) 425.
24. E. Gómez, E. Pellicer, E. Vallés, *J. Solid State Electrochem*., 8 (2004) 497.
25. E. Gómez, E. Pellicer, E. Vallés, *J. of Electroanalytical Chem*., 580 (2005) 238.
26. E. Gómez, E. Pellicer, E. Vallés, *J. of Electroanalytical Chem*., 517 (2001) 109.
27. E. Gómez, E. Pellicer, E. Vallés, *J. of Electroanalytical Chem.*, 556 (2003) 137.
28. G. Sandman, H. Dietz, W. Plieth, *J. of Electroanalytical Chem.*, 491 (2000) 78.
29. H. Cesiulis, N. Tsyntsaru, A. Budreika, N. Skridaila, *Surface Engineering and Applied Electrochemistry*, 46 (2010) 406.
30. J. Moulder, *Handbook of X-ray photoelectron spectroscopy*, Perkin-Elmer Corp., Minnesota (1992).
31. X. Duan, G. Qiaj, X. Zhou, *Chemical Engineering Journal*, 207 (2012) 103.
32. F. Liu, J. Arhancet, J. Coleman, M. McGrath - *US Patent* 7,932,419, 2011.
33. V. Talrose, E.B. Stern, A.A. Goncharova, N.A. Messineva, N.V. Trusova, M.V. Efimkina, *The NIST WebBook*, CAS: 108-95-2, (10-12-2012).
34. V. Talrose, E.B. Stern, A.A. Goncharova, N.A. Messineva, N.V. Trusova, M.V. Efimkina, *The NIST WebBook*, CAS: 71-43-2, (10-12-2012).
35. V. Talrose, E.B. Stern, A.A. Goncharova, N.A. Messineva, N.V. Trusova, M.V. Efimkina, *The NIST WebBook*, CAS: 110-82-7 (10-12-2012).